Scale resolving simulations of coherent unsteadiness over a benchmark configuration at a subcritical Reynolds number

Cite as: AIP Conference Proceedings **2223**, 020004 (2020); https://doi.org/10.1063/5.0000917
Published Online: 06 April 2020

Hariyo P. S. Pratomo

Scale Resolving Simulations of Coherent Unsteadiness over a Benchmark Configuration at a Subcritical Reynolds Number

Hariyo P. S. Pratomo[1,a)]

[1]*Department of Mechanical Engineering, Petra Christian University*
Siwalankerto Street 142-144, Surabaya 60236, Indonesia

[a)]hariyo_p@petra.ac.id

Abstract. Within the framework of eddy-resolving simulation, this paper aims to study the potential of two advanced turbulence modeling approaches in resolving turbulence scales over a reference geometry. Two *k-ω* SST based-scale resolving schemes are applied on a circular cylinder with a splitter immersed in turbulent flow at a sub-critical Reynolds number of around 3 x 10^4. The scale resolving computations starts with RANS predictions using the SST model where spatial and temporal grid studies are to be performed to craft the numerical mesh resolution required. With a standard *k-ω* SST model the results of the spatial and temporal grid sensitivity studies on the 2D domain give optimum mesh and timestep size to demonstrate the Strouhal number of 0.238 and unsuppressed vortex shedding after the rigid splitter. The vortex shedding phenomenon was also proven in an experimental study with a similar Reynolds number and equivalent ratios of splitter thickness and length to the cylinder diameter of 0.09 and 2.72, respectively. Under the optimum mesh and timestep size, comparison of the Strouhal number on 2D and 3D domains with one of the experiment is also performed, serving as a baseline point to modify the production of turbulent kinetic energy term in the k-transport equation of the standard *k-ω* SST model in order to evade an excessive generation of the turbulent kinetic energy due to the existence of a stagnation region ahead of the cylinder. On the 3D domain with the numerical ingredients, the computational results obtained with a modified *k-ω* SST model provide an encouraging result closer to the experimental data, giving the Strouhal number of 0.234. To study the inherent strategies in the two vorticity resolving schemes, the highest levels of the spatial and temporal grids are used. This is crucial to detect whether or not the finest mesh is prone to a numerical problem in one of the scale resolving formulations. During this stage, the ratio of the grid length scale to the RANS integral length scale, which is the functions of the turbulent kinetic energy and dissipation, in critical regions is scrutinized to be less than 0.1 – 0.2 to maintain high-quality mesh. The numerical results from the modified *k-ω* SST based-hybrid RANS-LES proposals suggest a prospective approach based on the modification of the dissipation term in the k-transport equation to be used even with a coarser grid, which is able to resolve turbulence scales on the configuration. The Strouhal number of 0.189 predicted by the superior model is close to a reference value in the experiment. The weakness and strategy in each scale resolving scheme are discussed within the context of crucial issues in the progress of the non-zonal hybrid RANS-LES models.

INTRODUCTION

Computational engineers are nowadays fortunate with the advent of scale resolving schemes which have the capability to surmount weaknesses in the accuracy of Reynolds Averaged Navier Stokes (RANS) solution and the expensive computational effort of Large Eddy Simulation (LES) for turbulence computation. The vorticity resolving methods are able to produce a reliably reduced eddy viscosity μ_t by increasing the dissipation rate of the turbulent kinetic energy *k*, i.e. the *ε*-term, or the specific dissipation rate of the turbulent kinetic energy *k*, that is the *ω*-term; in the formulation of the viscosity through an introduction of extra source term or a modification of the dissipation rate terms, i.e. the *ε*-term or the *ω*-term, contained in a turbulence transport equation of RANS model. Furthermore, the advanced approaches activate the RANS computation in the near-wall region and at the same time start the LES like-mode outside of the boundary layer region. Introducing a new turbulence length scale resided in the additional source

International Energy Conference ASTECHNOVA 2019
AIP Conf. Proc. 2223, 020004-1–020004-10; https://doi.org/10.1063/5.0000917
Published by AIP Publishing. 978-0-7354-1982-7/$30.00

term to build up the ω-term or initiating the RANS calculation within the boundary layer region with a relatively coarser grid than one of LES eventually will lessen the extravagant computation of LES. However, this introduces the daunting task to select an appropriate technique for different cases as the turbulence is case dependent. Technically, the scale resolving scheme is also widely known as a hybrid RANS-LES formulation that unites the strengths of the RANS and LES modes.

Various hybrid RANS-LES models emerge from its first conception in 1997. At that time the computational engineers were introduced to Detached Eddy Simulation (DES) of Spalart et al [1]. In principle, the hybrid methods are capable of resolving turbulence scales and maintaining the more affordable computation at practical Reynolds numbers than Direct Numerical Simulation (DNS) along with standard LES calculation. Within the hybrid approach, one can mention for example Delayed Detached Eddy Simulation (DDES) of Menter and Kuntz [2], Scale Adaptive Simulation (SAS) of Menter and Egorov [3], Spalart-Allmaras Zonal Detached Eddy Simulation (S-A ZDES) of Deck [4], RANS-Implicit Large Eddy Simulation (RANS-ILES) of Islam and Thornber [5]. In the hybrid proposals, we can categorize them into zonal and non-zonal techniques. In the zonal method, the user decides the predefinition of the LES and RANS regions prior to the execution of the simulation through the grid design, the determination of an explicit border, or the selection of domains not especially related to the wall regions [6]. Conversely, in the non-zonal or global technique, the method itself automatically chooses the simulation mode during the run, and thus the predefinitions between RANS and LES regions are avoided before the computation, according to Breuer et al [6].

Throughout this paper, the focus is restricted to the non-zonal hybrid RANS-LES formulation as the method is more practical and straightforward than the zonal counterpart with respects to reduced efforts from the user side on intuitively judging different turbulence regions that are manifested through the grid design. From the above-mentioned exemplars, SAS of Menter and Egorov [3] and DDES of Menter and Kuntz [2] are in the non-zonal group and accessible from various fluid solvers such as ANSYS Fluent®, ANSYS CFX®, Autodesk CFD®, OpenFOAM®. Moreover, those two-hybrid approaches are based on the *k-ω* SST model of Menter et al [7] as the baseline RANS formulation. Applications of the SAS and DDES methodologies can be found in the literature ranging from simple and complex configurations. The readers are referred to SAS computations, for example, onto periodic hill, military airplane, and rectangular shallow cavity in Menter et al [8], the Vattenfall test case T-junction in Frank et al [9], 3D-bubble column of Deen [10] in Massod et al [11], direct injection spark ignition engine in Theile et al [12] as well as DDES simulations onto wall-mounted hump, NACA0021, near wake of a cylindrical forebody in Guseva et al [13], control valve with T-junction in Wang et al [14]. The numerical results in the former studies [8,9,11,12], Guseva et al 2017 [13], Wang et al 2018 [14] have proven the capabilities of the scale resolving schemes to produce vorticity scales with varying degrees of success. In the SAS model the von Karman length scale L_{vK} allowing the method to adjust to turbulence scales in the computation which is not explicitly dependent on the spatial mesh resolution and automatically reducing the eddy viscosity μ_t in certain regions to the appropriate LES level if the grid permits are the crucial factor [8]. Unlike the SAS approach, within the DDES formulation the decisive elements are the ratio of the RANS integral length scale l_t to a variant length scale comprising a DES constant C_{DES} and filter width Δ which is explicitly dependent on the mesh resolution and a shielding function to defend the activations of the RANS and LES modes in desired regions and to diminish the eddy viscosity μ_t [8].

As per the author's knowledge, it is the first time that the *k-ω* SST SAS and *k-ω* SST DDES proposals have been employed to simulate a new benchmark of De Nayer et al [15], Kalmbach [16] in this new study where a flexible thin plate attached at the rear of a fixed circular cylinder is treated as a rigid splitter before proceeding with a multiphysics computation using a prospective hybrid model between those two. Physically, under a sub-critical Reynolds number the configuration studied poses transition in shear layers and the effect of their interactions in the wake region of the test case, which results in unsuppressed vortex shedding behind the body. These distinctive phenomena are reported in the experimental study of Apelt and West [17] where their problem geometry and Reynolds number are similar and have akin ratios of plate thickness and length to the diameter of a cylinder with ones used in this present study. This, therefore, brings the impetus to examine the performance of the *k-ω* SST SAS and *k-ω* SST DDES approaches on the aerodynamics test case in that: *how do the inherent strategies in those two-hybrid formulations respond to the distinguishing phenomena associated with flow instability in order to predict the turbulence over the geometry?* Additionally, in the context of fluid-structure interaction (FSI), an interplay between fluid flow and moving or deforming solid, the capacities of the SAS and DDES techniques also have not yet been investigated within the coupled computations of the proposed test case of De Nayer et al [15] and Kalmbach [16] where the splitter is replaced with a rubber for the FSI simulation. An intriguing inquiry in this circumstance is *how the innate methods of the SAS and DDES methodologies predict the turbulence developed over which simultaneously interacts with a moving and deforming structure*. Several previous FSI studies of De Nayer et al [15], Ali [18], and Kondratyuk [19] with the Smagorinsky LES, *k-ε-ζ-f* DDES, *k-ε* Very Large Eddy Simulation (VLES), and *ζ-f* VLES proposals have concluded

the performances of the corresponding eddy-resolving techniques on the FSI benchmark although under-predictions of the oscillation of the rubber were found in the coupled computations with the *k-ε-ζ-f* DDES, *k-ε* VLES, *ζ-f* VLES models as reported by Ali [18] and Kondratyuk [19]. As compared to the *k-ω* SST SAS and *k-ω* SST DDES methodologies, the *k-ε-ζ-f* DDES, *k-ε* VLES, *ζ-f* VLES approaches essentially have different strategies in the baseline RANS model used, the definition of the resolution control function called as the length scale ratio or the hybrid function, and in the formulation of the shielding function to circumvent the Grid Induced Separation (GIS), a crucial term in the hybrid RANS-LES simulation coined by Spalart et al [20]. For further details in the formulation, the readers are referred to Ali [18] and Kondratyuk [19].

METHODOLOGY

Before the run of transient pure flow computations with SAS of Menter and Egorov [3] and DDES of Menter and Kuntz [2], several methodological procedures as the pivotal basis for the success of the eddy-resolving simulations have to be performed. This includes spatial mesh convergence study and time sensitivity analysis with the *k-ω* SST model on a 2D domain, transient flow simulations with a modified *k-ω* SST formulation on the 3D domain as well as the modified *k-ω* SST SAS and modified *k-ω* SST DDES computations on 3D domains with a LES quality mesh. In the transient simulations with the eddy-resolving methodologies, the *k-ω* SST model of Menter et al [7] ingrained in the hybrid modeling approaches functions as the baseline RANS method. This means that if the turbulent flow is weakly unstable in the fluid domain then the scale resolving schemes will return back to RANS solution. The SST model is preferred in this new study as the method gives accurate predictions of the onset and the amount of flow separation under adverse pressure gradients and accounts for the transport of the turbulent shear stress. Detailed formulations of the turbulence transport equations for the turbulent kinetic energy *k* and the turbulent frequency *ω* and the eddy viscosity μ_t in the *k-ω* SST model are given in Menter et al [7].

Besides the distinctive phenomena as explained above, the existence of a stagnation region in front of the benchmark configuration investigated in this present study has to be treated properly. In essence, the stagnation region will cause excessive production of the turbulent kinetic energy *k*. As a result, the production of the turbulent kinetic energy *k*, i.e. the P_k-term, in the *k*-transport equation of the SST model has to be corrected by a production limiter. The definition of the production control follows Menter [21] and reads

$$P_k = min(P_k, C_{lim}\rho\varepsilon) \tag{1}$$

In equation (1), the *min* is a numerical function that yields the numerically smallest value between P_k and $C_{lim}\rho\varepsilon$ in the computational domain. The correct functionality of $C_{lim}\rho\varepsilon$ is protected by $C_{lim}\rho\varepsilon$ in the computational domain. The correct functionality of $C_{lim}\rho\varepsilon$ is protected by C_{lim} that is a clip coefficient. For the *k*-ω SST formulation, the clip coefficient is set to 10 according to ANSYS [22]. Applying equation (1) to the P_k-term in the *k*-transport equation of the SST model, a modified SST formulation holds. This modified SST model is consistently used in the SAS and DDES computations as the baseline RANS approach.

Within the modified *k-ω* SST DDES formulation, reduction in the eddy viscosity μ_t is realized through alteration in the dissipation term of the turbulent kinetic energy *k*: the *ε*-term in the *k*-transport equation of the DDES formulation [2]. This is associated with the presence of hybrid function F_{DDES} in the dissipation term, i.e. the *ε*-term. The modification is defined as in (2)

$$\beta^* k\omega F_{DDES} = \beta^* k\omega \, max\left(\frac{l_t}{C_{DES}\Delta}(1 - F_{SST}), 1\right) \tag{2}$$

In (2), the multiplier or hybrid function F_{DDES} is a length scale limiter which contains the RANS turbulence length scale l_t computed by the modified SST model, LES like-length scale $C_{DES}\Delta$, and blending functions F_{SST} of the SST method. In the equation, C_{DES} is a constant and Δ is filter width. The filter width or grid spacing Δ allows the eddy-resolving method to produce LES like-solution in certain regions when $C_{DES}\Delta \leq l_t$ is satisfied. In the DDES methodology, the grid spacing is expressed as

$\Delta \equiv \max(\Delta_x, \Delta_y, \Delta_z)$

$$\Delta \equiv \max(\Delta_x, \Delta_y, \Delta_z) \tag{3}$$

where Δ_x, Δ_y, and Δ_z are the grid spacing in the x, y, and z directions, respectively. Also, to provide a strong shielding to the RANS mode in the near-wall or boundary layer region, the SST blending function F_{SST} is set to F_2 which is the second blending function of the SST approach. The second blending function is defined according to Menter [21]. The transport equation of the turbulence frequency ω, i.e. the ω-transport equation, of the DDES method is similar to one of the SST models.

Unlike the DDES technique, the inborn strategy of the k-ω SST SAS formulation to lower the eddy viscosity μ_t is different. In the SAS approach of Menter and Egorov [3], the turbulent eddy viscosity μ_t is lessened by revising the transport equation of the turbulence frequency ω in the SST model. This is done via the introduction of a supplementary source term Q_{SAS} that is a function of the shear strain rate tensor **S**, the length scale L, the von Karman length scale L_{vK}, the turbulent kinetic energy k, and the turbulence frequency ω. The source term Q_{SAS} and the von Karman length scale L_{vK} are formulated in (4) and (5). Interestingly, there is no filter width variable Δ in the definition of the extra term Q_{SAS}. Such an approach is safer than one of the DDES model from the attack of GIS when the mesh refinement in certain regions is indispensable. Nevertheless, the functionality of the additional term Q_{SAS} is strongly affected by the flow variables where the key variables in the Q_{SAS} definition are the von Karman length scale L_{vK} and the shear strain rate tensor **S**. For this reason, when the new term Q_{SAS} is zero, owing to the calculation of those two flow solutions, then the ω-transport equation returns back to its original form of the SST model. This means that the vortex scales can not be resolved by the SAS method.

$$Q_{SAS} = max\left[\rho\zeta_2\kappa S^2\left(\frac{L}{L_{vK}}\right)^2 - C\frac{2\rho k}{\sigma_\varphi}max\left(\frac{1}{\omega^2}\frac{\partial\omega}{\partial x_j}\frac{\partial\omega}{\partial x_j}, \frac{1}{k^2}\frac{\partial k}{\partial x_j}\frac{\partial k}{\partial x_j}\right), 0\right] \tag{4}$$

$$L_{vK} = \frac{\kappa S}{|U''|} \tag{5}$$

In (5), U'' is the second velocity derivative. Likewise, the k-transport equation in the SST method, the corresponding transport equation of the SAS scheme is identical.

As turbulent flow over the test case demonstrates flow separation, transition in shear layers, and vortex shedding, good mesh resolutions are required in certain regions, i.e. the near-wall regions along the cylinder and splitter, wake and downstream regions. A correct beginning of the flow separation on the geometry is critical in which directly affects the size of the wake region. Bearing these important issues in mind, three levels of mesh resolution, i.e. coarse, medium, and fine, are designed on 2D domains for the convergence and sensitivity studies where the near-wall y^+ spacing is maintained to be around 1 and an automatic wall function [21] is used. For the transient flow computations with the modified k-ω SST SAS and modified k-ω SST DDES approaches the LES quality grid of 14,394,528 control volumes is exercised, having the properties of $\Delta y^+ < 5$, $\Delta x^+ = 40$, $\Delta z^+ = 64$, and growth rate = 1.05 where the ratio of the maximum grid length along the geometry h_{max} to the boundary layer thickness δ is crafted to be less than 0.5 – 1. The boundary conditions for the RANS computations include inlet, outlet, no-slip walls for the cylinder and thin plate, and slip walls for upper and lower walls, and symmetries for lateral walls while for the scale resolving simulations the boundary conditions comprise inlet, outlet, no-slip walls for the solids, slip walls for the upper and lower walls, and periodicity for the lateral walls. Both the RANS and hybrid scheme computations exploit RANS turbulence inlet for the inlet boundary conditions.

After unsteady flow simulations using the statistical turbulence modeling approaches are accomplished then transient flow computations with the modified k-ω SST SAS method and modified k-ω SST DDES model are performed. Following Garcia-Villalba et al [23], two monitoring points for the turbulent kinetic energy k are added in the wake region behind the circular cylinder, as illustrated in Fig. 3, to observe the evolution in time of the turbulent kinetic energy k for the requirement of non-dimensional advection time t^*, defined as $\{(t.U_{inflow})/D\} > 100$. Following this settlement time phase, the transient statistics averaging period is subsequently started. After the t^* requirement is accomplished, the statistics averaging procedure is carried out within the non-dimensional convection time of 200 to gauge the frequency f of velocity with the Fast Fourier Transform (FFT). With this, the Strouhal number St defined as $(fD)/U_{inflow}$ can be evaluated and compared with a reference value from an experiment of Apelt and West [17]. In this study, D in the Strouhal number equation is the diameter of the circular cylinder. The monitoring point for the velocity in the numerical simulations is located in the wake region and on a middle plane of the computational domain. In the 3D unsteady computations, subset domains are used as two-point correlations dropped towards zero value within the subset domain [24].

Time integration in the non-zonal hybrid RANS-LES simulations with the SAS and DDES formulations employ the Bounded Central Difference (BCD) scheme of Jasak et al [25] for the discretization of the convection terms. The

BCD approach is less numerically dissipative than the Second Order Upwind scheme with a blending factor, i.e. the High-Resolution approach developed for the RANS calculation and more dissipative than the Central Difference (CD) method but is stable and does not produce an unphysical oscillating solution. Within the transient flow simulations with the SAS and DDES models, the Courant-Friedrichs-Lewy (CFL) condition is kept to be equal to unity, resulting in a fine timestep size Δt of 2.5 x 10^{-5} seconds. To this, an implicit time integration scheme which is the second-order backward Euler is exercised for the temporal discretization. The implicit backward Euler approach is extensively accepted to have sufficient accuracy for widespread applications.

RESULTS AND DISCUSSION

The numerical results of the mesh convergence study on the 2D domain with the standard k-ω SST model are recapitulated in Table 1. Within the transient simulations in the convergence study, a timestep size Δt of 1.25 x 10^{-4} seconds is exploited, corresponding to the maximum CFL number of 1 in the fluid domain.

Comparing the numerical values of the Strouhal number St that are in a range of the asymptotic behavior, i.e. between 0.238 and 0.241 in Table 1, with the reference Strouhal number of 0.18 in Apelt and West [17] on Table 2, the difference in the results is quite large. This is because of the excessive generation of the turbulent kinetic energy k in the stagnation region, the accuracy of the RANS method, and a thin spanwise direction-3D domain, i.e. a 2D domain employed in the unsteady simulation for the RANS prediction which is advantageous on the expense of the computational effort with a reduced size in the control volume. Still, the grid convergence study does benefit for the design of the 3D computational mesh within the non-zonal hybrid RANS-LES simulations with the SAS and DDES methodologies on a LES quality mesh depicted in Fig. 1 and successfully replicates unsuppressed vortex shedding as found by Apelt and West [17]. The von Karman vortex shedding phenomenon from the computations is illustrated in Fig. 2. After the spatial grid independence procedure, an optimal time step size Δt of 0.002 seconds is obtained from the time-sensitivity analysis with the standard k-ω SST model on the optimum mesh of 97,674 control volumes. This sensitivity analysis is performed with seven levels of the timestep size Δt, starting from the finest size of 1.25 x 10^{-4} seconds to the coarsest level of 0.004 seconds.

TABLE 1. Mesh independence study with the standard k-ω SST model on the 2D domain.

Mesh size (control volume)	Strouhal number, St	Grid size, h (m)	Refinement factor, r	Solution difference, ε	Convergence order, p	Extrapolated value, ϕ	Approximated relative error, e_a (%)	GCI (%)
23,250		0.0024						
47,670	0.232	0.0019	1.27					
97,674	0.238	0.0015	1.27	-0.006		0.243	2.232	2.836
199,924	0.241	0.0012	1.27	-0.003	4.768	0.243	1.518	0.905

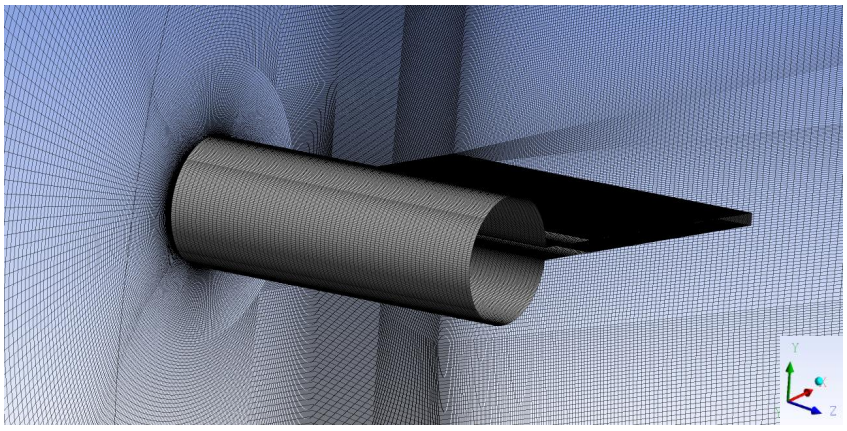

FIGURE 1. LES quality mesh resolution of 14,394,528 control volumes for the SAS and DDES computations: $y^+ \approx 1$, $\Delta y^+ < 5$, $\Delta x^+ = 40$, $\Delta z^+ = 64$, and a growth rate of 1.05 with $(h_{max}/\delta) < 0.5 - 1$.

Subsequently, with the grid resolution of 97,674 control volumes, a 3D mesh is developed by extruding the computational domain into the spanwise direction to meet the size of a subset domain in De Nayer et al [24]. In this case, the grid spacing is evenly distributed in the lateral direction, giving 18 equidistant spanwise cells. Using the standard k-ω SST and modified k-ω SST formulations the unsteady flow computations are performed on the mesh size of 1,758,132 control volumes with the timestep size Δt of 1.25 x 10^{-4} seconds within a total simulation time of 4 seconds. The corresponding numerical results are summarized in Table 2. It is demonstrated that the modified k-ω SST model can improve the Strouhal number from 0.244 to 0.234 in comparison to the standard k-ω SST method which results in the Strouhal number of 0.238. Again, the difference in the results is still far from the referenced Strouhal number of 0.18 as in Apelt and West [17]. This is the case for the RANS prediction associated with the weakness in its accuracy owing to the intrinsic strategy in the RANS method regardless of the production limiter used to avoid the immoderate generation of the turbulent kinetic energy k in the stagnation region.

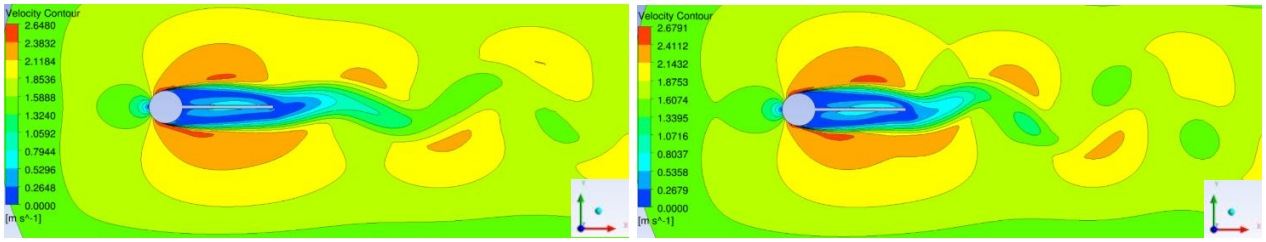

(a) mesh size of 97,674 control volumes (b) mesh size of 199,974 control volumes

FIGURE 2. Averaged velocity contours captured at 2.5 seconds produced from transient simulations with the standard k-□ SST model.

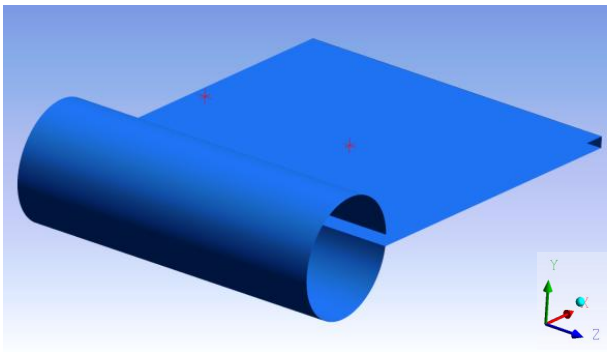

FIGURE 3. Two monitoring points of the turbulent kinetic energy k located in the wake region for the transient flow simulations with the modified k-ω SST SAS and modified k-ω SST DDES formulations.

Following the RANS computations on the 3D flow domain, the transient flow simulations are extended to ones with the modified k-ω SST SAS and modified k-ω SST DDES methods. The LES mesh utilized is crafted from the finest 2D mesh of 199,924 control volumes with an extrusion into the lateral direction to produce the subset domain with 72 equidistant cells. On this basis, the LES mesh has multiple practical purposes. Firstly, within the SAS computation, the LES grid resolution is the key modality to correctly produce the shear strain rate tensor **S** which is sensitive to the flow instability in the domain. As in (4) and (5), the strain rate tensor, **S**, is the sole element to safeguard the functionality of Q_{SAS} to be non-zero. Secondly, in the DDES simulation, the LES grid will authorize the filter width Δ to produce LES like-solution in certain regions. In particular, to the ratio of h_{max}/δ, the LES mesh is an apt media to examine the protection of the second blending function of the SST model F_2 to the correct activation of RANS mode in the near-wall region and against the attack of GIS.

During the course of the non-zonal hybrid RANS-LES computation, steady k-ω SST solutions are used as initialization for subsequent transient simulations with the SAS and DDES techniques. To let the turbulent flow over the benchmark be settled during a starting time, the evolutions of the turbulent kinetic energy k in time are monitored until the non-dimensional advection time t^* of more than 100. After this point, the transient averaging procedure is

activated and finished within the convection time t^* of 200. The monitor of these evolutions in time is illustrated in Fig. 4.

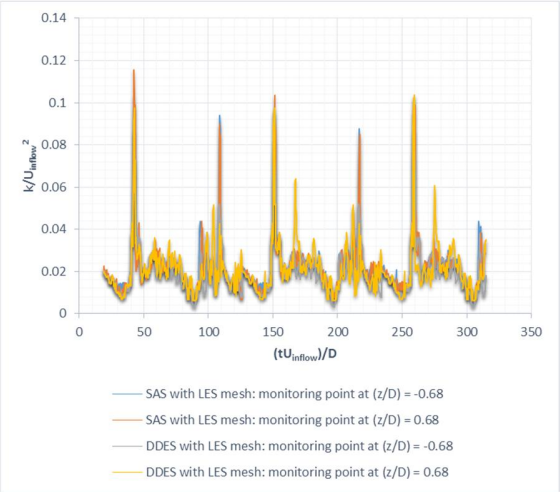

FIGURE 4. Evolutions of the turbulent kinetic energy k in time within the non-dimensional advection time t^* of more than 300 measured by the modified k-ω SST SAS and modified k-ω SST DDES techniques.

Figure 5(a) shows the eddy scales produced by the modified k-ω SST-SAS approach. The turbulence scales are captured at the advection time t^* of 125. It is clear from the figure that the SAS model fails to sufficiently resolve the vorticity scales on the geometry, even on the LES mesh and the very small timestep size Δt of 2.5 x 10^{-5} seconds corresponding to the CFL number of less than 1 [24]. The scale resolving simulation on the test case just produces a RANS like-solution. In this case, even with a different non-dissipative convection scheme, i.e. the Central Difference Scheme, and eddy viscosity limiters such attempts also do not offer any helps, as reported by Pratomo and Schäfer [26]. The fine mesh resolution simply produces the shear strain rate S and the von Karman length scale L_{vK} that eventually neglect the additional source term Q_{SAS}. Obviously, even though the flow is unstably associated with the unsuppressed von Karman vortex shedding as in Fig. 2, the shear strain rate S in the wake region is high due to the existence of the splitter as shown in Fig. 5(b) with the red color. The Strouhal number St evaluated from the SAS technique is summed up in Table 2. Based on this, the capability of the SAS method to resolve the unsteady scales thus relies on the production of the shear strain rate S which is case dependent and affected by proper grid resolution in the sense of numerical simulation. Returning back to the failure of the SAS technology in capturing the complex vortex scales, the turbulent flow over the benchmark can be said to be weakly unstable.

Figure 6 illustrates the vorticity scales produced by the modified k-ω SST-DDES method. The turbulence scales are captured at the advection time t^* of 125. Compared to the SAS approach, the DDES model is more superior than the SAS model. With the LES mesh and the extremely fine timestep size Δt of 2.5 x 10^{-5} seconds, the DDES methodology is able to resolve the eddy scales on the configuration. Nevertheless, the transition in shear layers just near to the apex of the cylinder can not be reproduced by this technique. Thus, the coherent structures just behind the cylinder are different as compared to visualization made by Apelt and West [17]. In the sense of numerical simulation, this is due to the definition of the grid spacing or filter width Δ as in equation (3) which is the sole function of the grid spacing. In (3) uses the numerical function of *max* yielding the numerically biggest value between grid spacing in the x-direction Δ_x, grid spacing in the y-direction Δ_y, and grid spacing in the z-direction Δ_z in the computational domain. Such a scenario can be problematic as the vorticity scales-resolution in shear layers not only depends on the grid spacings without any correction but also on flow parameters. Concerning this, a number of researchers quite recently have proposed various definitions in the filter width Δ. For instance, one can mention Guseva et al [13] who introduced a new formulation in the definition of the filter width Δ based on a shear layer adaptation. Essentially, the weakness in the transition resolution as previously explained nowadays is related to a solidly desired attribute of the hybrid RANS-LES model in providing a fast transition from RANS to LES solution as explained by Shur et al [27]. To mitigate this problem, one can alter the formulation of the filter width Δ by introducing the novel expression of Guseva et al [13] for the grid spacing, i.e. a shear layer adapted-filter width Δ_{SLA}. With the new definition in the grid length size, Δ_{SLA}Guseva et al [13] reported the aggressive performance of a new DDES method onto a wall-mounted hump;

thus improving the capability of the DDES model based on the standard filter width Δ as in (3). The Strouhal number *St* examined from the DDES approach is recapitulated in Table 2, providing a value of 0.189 which is close to the reference of 0.18. Furthermore, the contour of the second blending function F_2 of the SST model in the DDES computation is demonstrated in Fig. 7. From the Fig. 7, it is clearly seen that the SST blending function F_2 can provide strong protection to shield the boundary layer region. Therefore, this evades the attack of GIS as the near-wall region is colored with red, having the number of 1. This means that the RANS mode is active in the whole location. Moreover, all the converged solutions in the SST, SAS, and DDES computations are obtained with an RMS convergence criteria of less than 10^{-4}.

TABLE 2. Comparisons between the present numerical results and experimental reference of Apelt and West (1975) on a 3D computational domain.

Parameter	**Present numerical results (*h/D*) = 0.09 and (*L/D*) = 2.72**	**Experiment of Apelt and West (1975) (*h/D*) = 0.09 and (*L/D*) = 2.72**	**Remarks**
Strouhal number	0.244	0.18	standard *k-ω* SST model on the mesh size of 1,758,132 control volumes
	0.234		modified *k-ω* SST model on the mesh size of 1,758,132 control volumes
	0.227		modified *k-ω* SST SAS model on the mesh size of 14,394,528 control volumes
	0.189		modified k-*ω* SST DDES model on the mesh size of 14,394,528 control volumes

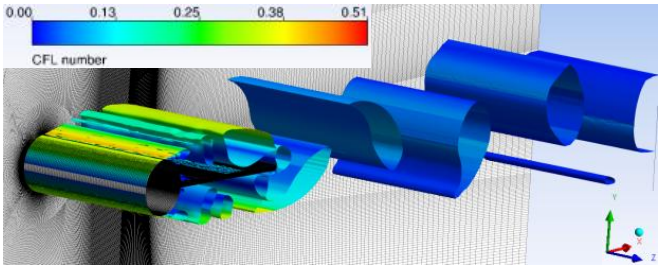

(a) Turbulence scales colored with CFL number from the Q-criterion

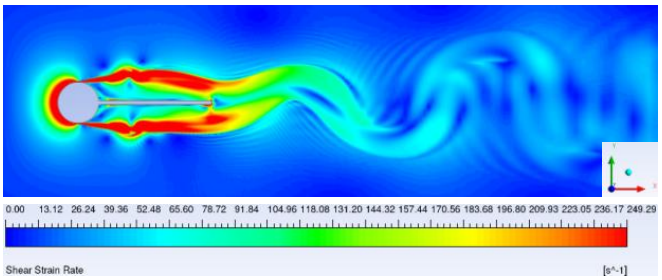

(b) The contour of the shear strain rate tensor

FIGURE 5. Results of the SAS computation on the LES mesh of 14,394,528 control volumes (reproduced from Pratomo and Schäfer [26])

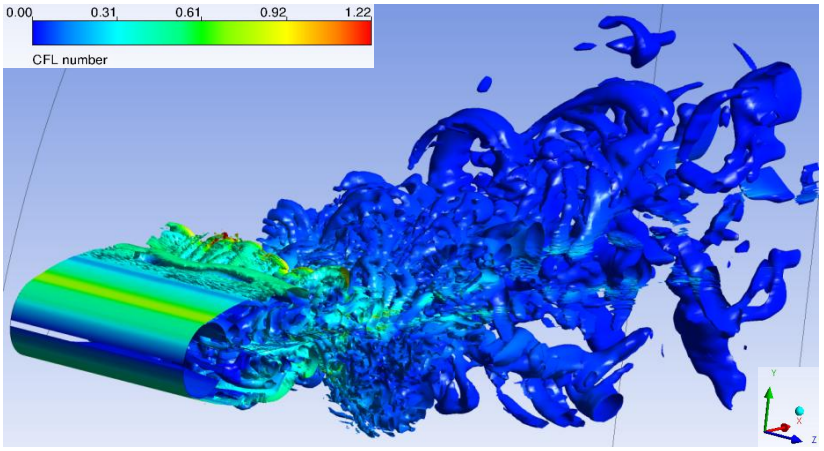

FIGURE 6. Turbulence scales resolved by the DDES computation on the LES mesh 14,394,528 control volumes

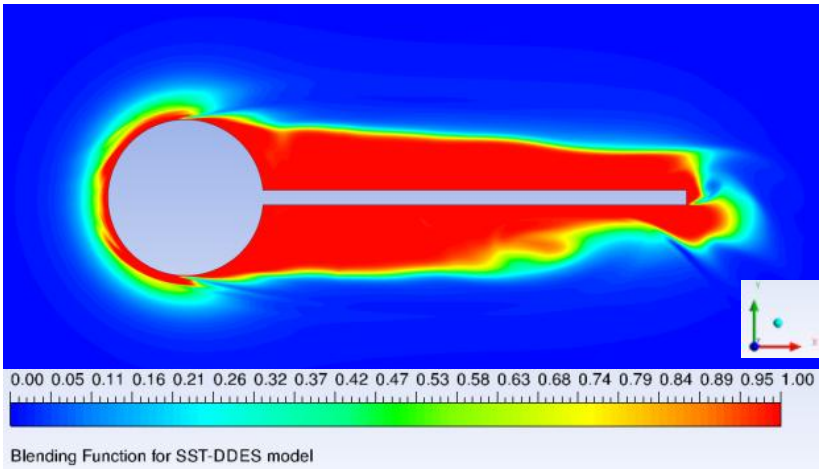

FIGURE 7. SST blending function used in the DDES computation on the LES mesh 14,394,528 control volumes

CONCLUSION

This paper aims to study the potential of two advanced turbulence modeling approaches in resolving turbulence scales over a reference geometry. Two modified k-ω SST based-scale resolving schemes are applied on a circular cylinder with a splitter immersed in turbulent flow at a sub-critical Reynolds number. With the RANS computations, it is evident that the RANS method suffers from the weakness in its accuracy owing to the inherent strategy used in the statistical modeling approach. This is well proven in the current numerical results on 2D and 3D domains. In the 3D transient flow computations with the LES mesh and CFL condition of around unity, the DDES formulation is found to be more superior than the SAS model for the turbulence prediction on the benchmark configuration. The complex eddy scales behind the configuration thus are successfully captured by the DDES model; unlike the SAS technique which fails to produce a large range of the turbulence scales. In principle, the success of the SAS method in resolving the vorticity scales is determined by the shear strain rate S which is sensitive to the dynamics of flow and contributes to the von Karman length scale L_{vK} in the extra source term Q_{SAS}. Lastly, the aggressive performance of the DDES formula to offer a rapid transition from RANS to LES solution can be improved by introducing a new definition in the filter width Δ instead of the standard filter width Δ utilized in this study.

ACKNOWLEDGMENTS

The author is indebted to Prof. Dr. rer. nat Michael Schäfer who has introduced and trusted him with the research in turbulence and fluid-structure interaction at Fachgebiet Numerische Berechnungsverfahren im Maschinenbau (FNB), Technische Universität (TU) Darmstadt and gratefully acknowledges the supports of the Lichtenberg High Performance Computer of TU Darmstadt for extensive computations in the research and the scholarships of Kementerian Riset, Teknologi, dan Pendidikan Tinggi Republik Indonesia and Universitas Kristen Petra. It is expressly stated that major parts of this manuscript have been prepared by the author during his doctoral study at FNB, TU Darmstadt. Finally, insightful comments from reviewers that have strengthened the manuscript as well as deep discussions with Mr. Martin Straka of Physikalisch-Technische Bundesanstalt (PTB) Berlin, Dr.-Ing. Wolfgang Bauer of ANSYS Germany and Institut für Land- und Seeverkehr – Fachgebiet Fahrzengantriebe of TU Berlin, and Abe H. Lee, Ph.D., graduate of the Pennsylvania State University, are also gratefully acknowledged.

REFERENCES

1. P. R. Spalart, W.-H. Jou, M. Strelets, and S. R. Allmaras, "Comments on the feasibility of LES for wings, and on a hybrid RANS/ LES," in *Advances in DNS/LES: Direct numerical simulation and large eddy simulation*, International conference, edited by C. Liu, Z. Liu, L. Sakell (Greyden Press, Ruston, LA, 1997), pp. 137 – 147.
2. F. R. Menter and M. Kuntz, "Adaptation of eddy-viscosity turbulence models to unsteady separated flow behind vehicles," in *Symposium on the aerodynamics of heavy vehicles: trucks, buses, and trains*, edited by R. McCallen, F. Browand, and J. Ross (Springer, 2004), pp. 339 – 352.
3. F. R. Menter and Y. Egorov, Flow Turbul. Combust. **85(1)**, 113 – 138 (2010**)**.
4. S. Deck, Theoret. Comput. Fluid Dyn. **26**, 523-550 (2012).
5. A. Islam and B. Thornber, Comput. Fluids **167**, 292 – 312 (2018).
6. M. Breuer, B. Jaffrézic, and K. Arora, Theoret. Comput. Fluid Dyn. **22(3)**, 157 – 187 (2008).
7. F. R. Menter, M. Kuntz, and R. Langtry, "Ten years of industrial experience with the SST turbulence model," in *Heat and Mass Transfer 4*, *4th International Symposium, Turbulence, Heat and Mass Transfer,* edited by K. Hanjalić, Y. Nagano, and M. Tummers (Begell House, Wallingford, NY, 2003), pp. 625 – 632.
8. F. R. Menter, J. Schuetze, and K. A. Kurbatskii. "Scale-resolving simulation techniques in industrial CFD" in *6th AIAA Theoretical Fluid Mechanics Conference* (AIAA, Honolulu, Hawaii, 2011), pp. 1 – 12.
9. Th. Frank, C. Lifante, H.-M. Prasser, and F. R. Menter, Nuclear Eng. and Design **240(9)**, 2313 – 2328 (2010).
10. N. Deen, "An Experimental and Computational Study of Fluid Dynamics in Gas-Liquid Chemical Reactors," Ph.D. thesis, Aalborg University, 2001.
11. R. M. A. Massod, Y. Khalid, and A. Delgado, Chem. Eng. J. **262**, 1126 – 1136 (2015).
12. M. Theile, E. Hassel, D. Thévenin, B. Buchholz, K. Michels, and M. Hofer, SAE Int. J. Engine **9(4)**, 2320 – 2336 (2016).
13. E. K. Guseva, A. V. Garbaruk, and M. Kh. Strelets, Flow Turbul. Combust. **98**, 2 (2017).
14. P. Wang, H. Ma, and Y. Liu, J. Fluids Eng. **140**, 8 (2018).
15. G. De Nayer, A. Kalmbach, M. Breuer, S. Sicklinger, and R. Wüchner, Comp. Fluids. **99**, 18 – 43 (2014).
16. A. Kalmbach, "Experimental investigations on vortex-induced fluid-structure interaction benchmarks and corresponding RANS predictions," Dr.-Ing. dissertation, Helmut-Schmidt Universität/ Universität der Bundeswehr, 2015.
17. C. J. Apelt and G. S. West. J. Fluid Mech. **71(1)**, 145 – 161 (1975).
18. A. Ali, "On the simulation of turbulent fluid-structure interaction," Dr.-Ing. dissertation, Technische Universität Darmstadt, 2017.
19. A. Kondratyuk, "Investigation of the Very Large Eddy Simulation model in the context of fluid-structure interaction," Dr.-Ing. dissertation, Technische Universität Darmstadt, 2017.
20. P. R. Spalart, S. Deck, M. L. Shur, K. D. Squires, M. Kh. Strelets, and A. Travin, Theor. Comput. Fluid Dyn. **20**, 181–195 (2006).
21. F. R. Menter, AIAA J. **32(8)**, 1598 – 1605 (1994).
22. ANSYS, "Turbulence and Wall Function Theory" in ANSYS CFX Solver Theory Guide (ANSYS, Canonsburg, 2017), pp. 89 – 90.
23. M. Garcia-Villalba, N. Li, W. Rodi, and M. A. Leschziner, J. Fluid Mech. **627**, 55 – 96 (2009).
24. G. De Nayer, A. Kalmbach, and M. Breuer, "Fluid-structure interaction in turbulent flow past cylinder/plate configuration I (First swiveling mode)", available at http://www.kbwiki.ercoftac.org/w/index.php/Abstr:UFR_2-13. (2016). [Acessed on 2 May 2016]
25. H. Jasak, H. G. Weller, and A. D. Gosman, Int. J. Numer. Meth. Fluids **31**, 431–449 (1999).
26. H. P. S. Pratomo and M. Schäfer. "Assessment of hybrid turbulence modeling approaches for fluid-structure interaction," 4th International Conference on Computational Engineering (Graduate School of Computational Engineering Technische Universität Darmstadt, Darmstadt, 2017).
27. M. L. Shur, P. R. Spalart, M. K. Strelets, and A. K. Travin, Flow Turbul. Combust. **95**, 709 – 737 (2015).